Chemical Science

Accepted Manuscript

This article can be cited before page numbers have been issued, to do this please use: S. Paul, S. ., A. Das, D. Moonshiram and J. Dasgupta, *Chem. Sci.*, 2026, DOI: 10.1039/D5SC05247E.

ROYAL SOCIETY OF CHEMISTRY

rsc.li/chemical-science

View Article Online
DOI: 10.1039/D5SC05247E

Vibrational Snapshots of Ultrafast C-H Bond Photoactivation inside a Water-soluble Nanocage

Sunandita Paul[1a], Shashi[1], Ankita Das[1b], Dooshaye Moonshiram[2], and Jyotishman Dasgupta[1*]

[1] Department of Chemical Sciences, Tata Institute of Fundamental Research, Mumbai, India

[2]Instituto de Ciencia de Materiales de Madrid Consejo Superior de Investigaciones, Científicas Sor Juana Inésde la Cruz 3, Madrid 28049, Spain

Current Affiliations:

[a]Department of Chemistry, The University of Chicago, Chicago, Illinois 60637, USA; and the James Franck Institute, The University of Chicago, Chicago, Illinois 60637, USA

[b]School of Chemistry, University of Birmingham, Edgbaston, Birmingham B15 2TT, UK

Materials and Correspondence should be addressed to J.D.;

[*]Email: dasgupta@tifr.res.in

View Article Online
DOI: 10.1039/D5SC05247E

ABSTRACT: Triggering C-H bond photoactivation reactions inside enzyme-like nanocavities will enable development of green methods to carry out selective organic transformations in water. Recently it was shown that host-guest charge transfer interactions inside water-soluble cationic nanocages can be used to drive ultrafast C-H bond photoactivation to catalytically form selective products in water via a sequential proton-coupled electron transfer (PCET) reaction. However, the primary structural events after light absorption that couple the electron and proton transfer steps during the PCET process has remained elusive, thereby limiting the diversity of Cage-confined photoredox catalysis in water. Here we employ structure-sensitive femtosecond stimulated Raman spectroscopy to track the PCET driven catalytic photoactivation of C-H bond in Cage-confined 5-(5-methylthiophene-2-yl)-thiophene-carbaldehyde (BTMC), and its subsequent selective oxidation to the corresponding aldehyde at room temperature in water. Resonance-selective Raman snapshots of the photogenerated radical cation reveal the rich vibrational dynamics of the bithiophene rings leading up to formation of a neutral radical at the methyl-carbon site while suggesting a kinetic heterogeneity of the deprotonation event. In combination with broadband transient absorption and solvent water kinetic isotope effects, we demonstrate a key role of the pre-organized water-cluster around the host-guest complex during the C-H bond photoactivation. Our work illustrates the significance of controlling the guest self-assembly inside the Cage to tune the rate of preorganized proton-transfer, and therefore opens a temporal framework for developing universal PCET-guided photoredox transformations in water.

KEYWORDS: Femtosecond Stimulated Raman Spectroscopy, C-H bond photoactivation, PCET, broadband transient absorption spectroscopy, organic catalysis in water

View Article Online
DOI: 10.1039/D5SC05247E

Introduction

The most fundamental detail of any chemical reaction lies in the intricate electronic and structural details of its bond-breaking and/or bond-making steps[1]. It has been chemists' dream to visualize the nuclear dynamics that drive product formation in well-known organic transformations[2-6]. Selective C-H bond activation[7-9] represents a grand chemistry challenge as it promises to allow atom economy during organic synthesis[10, 11]. Classically, C-H activation has been catalytically achieved at metal centers where ligand-to-metal charge transfer interactions (see Figure 1) play a crucial role in breaking the C-H bond[12, 13]. Recently, time-resolved X-ray absorption spectroscopy was used to resolve the orbital-based description of the ligand-to-metal charge transfer interactions[14]. It has been elaborated that such specific and preorganized metal-ligand charge transfer interactions are necessary for widely diverse C-H bond activation reactions[15].

An alternate way for executing any generic X-H (X= O, N, S or C atom) bond cleavage is through a combination of electron transfer (ET) and proton transfer (PT) steps in pre-organized donor-acceptor systems[16-18]. Confinement of redox complementary organic substrates inside a supramolecular host cavity allows for formation of host-guest donor-acceptor charge transfer interactions[19-22 23-25] (Figure 1). Recently, it was demonstrated that photoexciting such water-soluble host-guest complexes with prominent CT interactions can drive X-H bond-activation chemistry via a sequential proton-coupled electron transfer (PCET) mechanism[24, 25]. It was hypothesized that the pre-organized water molecules around the supramolecular nanocavities enable O-H and N-H bond cleavage reactions within ~900 fs and ~3 ps respectively, via

View Article Online
DOI: 10.1039/D5SC05247E

photoinduced PCET[24]. Using this conceptual framework, Das *et al*. reported that ultrafast C-H bond photoactivation within tens of picoseconds could be performed inside a cationic, water-soluble supramolecular host nanocavity[26]. With such a photoredox scheme, the first selective transformation of toluene to benzaldehyde under ambient conditions,[26] mimicking the typical enzymatic turnover in water was achieved. However, a clear understanding of all the primary light-induced events, especially the structural dynamics in such a complex nanocavity has remained a critical challenge. More specifically a comprehensive view of the reaction coordinate that drives the sequential photoinduced PCET process has remained elusive. Therefore, it is imperative to watch the non-equilibrium events driving the sequential PCET while providing an experimental test-bed for the theory proposed by Hammes-Schiffer and co-workers[27] on defining a single solvent fluctuation coordinate even for photoinduced PCET reactions[28]. Elucidation of this fundamental reaction coordinate(s) would consequently lead to a rational design principle for a universal scheme of driving PCET-guided photoredox catalysis in water.

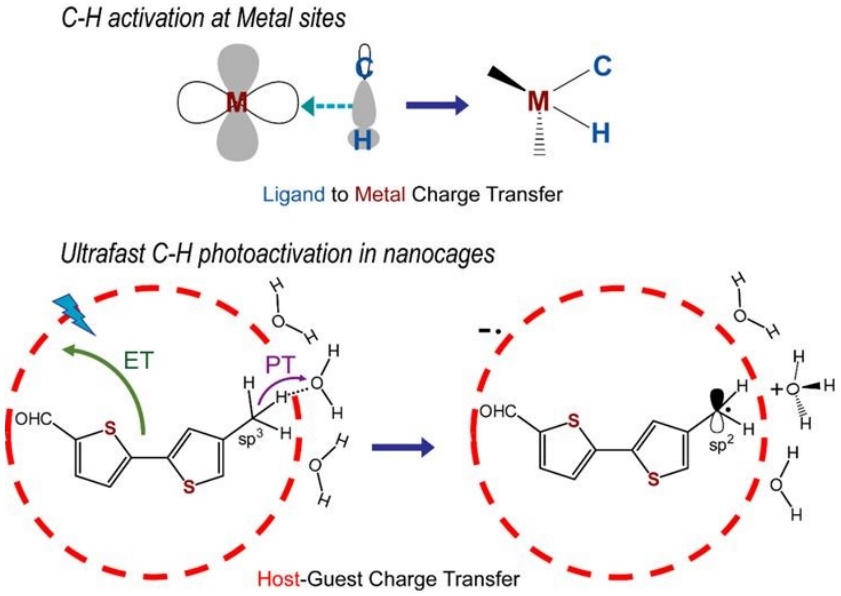

Figure 1: Conceptual figure depicting C-H activation routes. (top) The traditional C-H bond activation at metal sites; and (bottom) the novel host-guest charge transfer method for ultrafast photoactivation of the C-H bond. The fate of C-H bond for metal catalyst-based activation is the

View Article Online
DOI: 10.1039/D5SC05247E

formation of metal-carbon bond/ complex while for ultrafast photoactivation, a confined C-centered neutral radical is the transient product.

Ultrafast vibrational spectroscopy has been used to track structural changes accompanied during photoinduced bond breaking steps in many chemical and biological reactions[29-31]. For condensed phase reactions, time-resolved Raman in its variants has been hugely successful due to its selectivity of transient states via the resonance enhancement[32]. Compelling demonstrations of probing structural dynamics have been shown in diverse reactions such as CT reactions in conjugated polymers[33-35], photoisomerization reactions in proteins[36, 37] and excited state proton transfer reaction in GFP[38]. Additionally, in all these examples transient Raman spectroscopy enabled watching the reaction coordinate(s) which allowed for further tuning of the reaction efficiency of the chemical processes. Herein we use femtosecond stimulated Raman spectroscopy (FSRS)[39] to watch C-H bond cleavage reaction inside water-soluble nanocage for the first time, and interrogate the role of the pre-organized water cluster during the sequential photoinduced PCET process.

Substituted thiophenes as well as oligothiophenes of different chain length are highly useful for optoelectronic and photodynamic therapy applications although the fundamental organic transformations on the thiophene backbone are challenging due to their enhanced oxidative reactivity[40, 41].The paucity of selective C-H activation schemes for converting -CH_3 groups on thiophenes to reactive functional groups like aldehydes in one-step at room temperature are rare. To visualize the C-H bond cleavage, we chose 5-(5-methylthiophene-2-yl)-thiophene-carbaldehyde (BTMC) substrate which has a pendant CH_3 group (Figure 1) and confined it inside a water-soluble $Pd_6L_4^{12+}$ nanocavity[42]. Our choice of methyl-substituted bithiophene therefore was to provide a proof-of-concept C-H bond photoactivation reaction while exploiting the large Raman cross-section enabling sensitive visualization of photoinduced

View Article Online
DOI: 10.1039/D5SC05247E

structural dynamics. Incarceration of BTMC inside the host nanocage enables the generation of a visible host-guest CT state. Photoexcitation at the CT band triggers the C-H bond photoactivation step through the sequential proton-coupled electron transfer reaction. The whole reaction trajectory was probed in real-time using transient absorption and stimulated Raman spectroscopy which captured the radical cation and the neutral radical states through the changes at the methyl C-10 site. The FSRS spectral changes indicate that the proton transfer step occurs from the C_{10}-H bond to form a stable C-centred neutral radical, highly conjugated with the bithiophene backbone, and it has an electronic structure that equilibrates with the solvent shell in ~65 ps. The emergence of neutral radical like Raman features as early in tens of picoseconds in the FSRS data provides critical information about the significance of the orientational heterogeneity of the water cluster around the nanocage which drives the C-H bond photoactivation via sequential PCET. Our work, therefore, provides in-depth mechanistic view for the first example of a selective photo-catalytic oxidation of a methyl group to an aldehyde on a thiophene backbone in water under ambient conditions.

Results and Discussions

Host-Guest Complexation: The host cationic nanocage $Pd_6L_4^{12+}$ (L= tri-pyridyl-triazine; TPT) was synthesized by following the reported protocols[42] with some modifications (details of the synthesis has been provided in Supporting Information). The nanocage was characterized by carrying out ^{1}H-NMR spectroscopy to check the integrity of the self-assembled Cage (Figure S1). We prepared the host-guest complex by mixing 5-equivalents of BTMC in 2.5 mM aqueous solution of the Cage (see Figure 2a) and stirring the solution for 30 minutes. To check the incarceration of BTMC inside Cage, we carried out ^{1}H-NMR spectroscopy after filtering excess guest from yellow-coloured solution. Figure 2b shows the NMR spectra of BTMC⊂Cage in

View Article Online
DOI: 10.1039/D5SC05247E

D_2O. The peak marked in green comes from the molecule inside the Cage while the Cage protons (assignment in SI Figure S1) are marked in red. We see that all the guest protons are upfield shifted inside cavity as compared to the free molecule ^1H NMR spectra in $CDCl_3$ (Figure S2). The $-CH_3$ proton in BTMC⊂Cage comes at 1.26 ppm as compared to 2.51 ppm in free BTMC in $CDCl_3$. The unequivocal upfield shift can only be explained by the shielding effect of the cavity on the molecule. ^1H NMR binding titration was performed to study the host–guest complexation behaviour between the host Cage and BTMC guest. Increasing amounts of BTMC were added to 2.5 mM Cage in D_2O, and the ^1H NMR spectra were recorded. Slight changes in chemical shift values were seen for the Cage aromatic protons. Relative peak area integration in both host and guest protons indicated complex formation in 1:1 stoichiometry as shown in Figure S3 & S4.

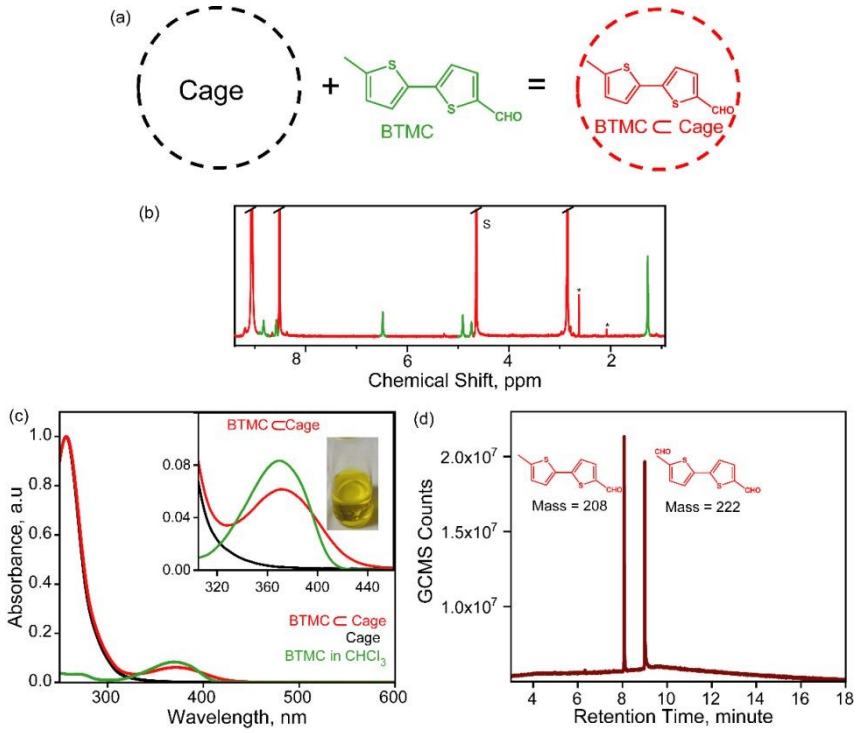

View Article Online
DOI: 10.1039/D5SC05247E

Figure 2: Characterization of Host-Guest Complex and Photo-redox Reaction. (a) Concept of incarceration of BTMC inside water soluble Cage. (b) NMR characterization of host-guest complexation. The green colored peaks denote the molecule NMR inside cavity. (c) Absorption of BTMC⊂Cage is shown (red trace) with comparison to free Cage (black trace) and BTMC in $CHCl_3$ (green trace). (d) GCMS trace showing product formation after photoreaction of BTMC⊂Cage.

Steady-state absorption measurements were done to characterize the optical features of the host-guest complex. Figure 2c shows the absorption of Cage (black trace), free BTMC molecule in $CHCl_3$ (green trace) and the host-guest complex (red trace) in the wavelength range from 240 nm to 600 nm. The free cavity in water shows an absorption maximum at 256 nm tailing to 380 nm. Free BTMC in $CHCl_3$ has an absorption maximum at 370 nm while it extends up to 420 nm (as shown in Figure S5). The host-guest complex of BTMC⊂Cage having a distinct yellow color has absorption features of both free cavity (maximum at 256 nm) and individual molecule absorption at 370 nm along with an extended band which now goes up to 450 nm (as shown in the inset of Figure 2c). The broadening of the absorption spectrum indicates the formation of a host-guest complex which leads to the intense yellow color of the solution. Previous work has shown that such extended absorption features can have charge transfer character[19, 24, 26] although in this case**,** the local excitations of the molecule could also be broadened due to Cage incarceration and heterogeneity of packing. However, it is unequivocal that the host-guest complex between an electron rich bithiophene molecule and the electron deficient Cage is stable, and can be photoexcited for carrying out C-H bond oxidation reaction as shown previously for toluene incarcerated in Cage[26].

Selective photoproduct upon visible light excitation: In order to test the C-H bond photoactivation reaction, we irradiated the aqueous solution containing 12.5 mM BTMC with 20 mol% Cage with 400 nm LED light (50 mW) source for 24 hrs. We observed the color change at the end of reaction while the photoproducts were extracted in $CHCl_3$ and analyzed by GCMS and

View Article Online
DOI: 10.1039/D5SC05247E

^{1}H NMR spectroscopy. Figure 2d shows the product distribution with the GC retention time. We observe only one product with a mass of 222 Da which was identified as the oxidized product, 2,2'bithiophene-5,5-carbaldehyde and also confirmed by ^{1}H NMR spectra (Figure S6 & S7). The formation of a single selective photoproduct via oxidative functionalization of the -CH_3 group to –CHO is analogous to the toluene oxidation to benzaldehyde [26]. It should be noted that such selective transformations in substrates with thiophene backbone has been challenging[43-45] . The mechanism to explain this oxidized product formation should therefore involve formation of a neutral radical on the -CH_3 group triggered by PCET driven C-H activation followed by reaction with dioxygen gas in ambient conditions[26, 46]. To confirm the role of oxygen in the photoreaction, we performed the reaction in both ambient and inert (under argon atmosphere) conditions. We found negligible product formation under inert conditions showing the role of oxygen in photo-oxidation as characterized by GCMS and ^{1}H NMR spectroscopy (SI figure S6 and S7). We also monitored the photoreaction in D_2O without extracting unreacted substrate and aldehyde photoproduct. The ^{1}H-NMR shows decrease in BTMC guest proton peaks, and appearance of new proton peaks corresponding to the product as shown in Figure S8 & S9. To confirm the photoinduced sequential PCET mechanism in case of BTMC⊂Cage complex, we have next performed transient absorption spectroscopy and FSRS.

Excited state dynamics of BTMC⊂Cage: To track the dynamics of potential radical intermediates at the -CH_3 site in BTMC after host-guest photoinduced charge transfer, transient absorption (TA) spectroscopy was carried out. Femtosecond transient absorption traces of BTMC⊂Cage subsequent to photoexcitation at 400 nm were recorded in both H_2O and D_2O. Figure 3a shows the TA traces in the probing window between 430 nm to 800 nm from negative100 fs to 300 ps in H_2O. We observe a rise in the excited state absorption feature (ESA)

View Article Online
DOI: 10.1039/D5SC05247E

having maxima at 458 nm till ~1 ps. Along with the sharp absorption feature, there is also a broad absorption feature throughout the visible region with lower oscillator strength up to 750 nm. Our TA feature matched with the known bithiophene radical cation spectra from previous flash photolysis experiments[47]. We, however, observed a slight red-shifted spectrum due to the additional[48] chemical appendages on the molecule such as the -CH_3 and –CHO moieties as well as being incarcerated inside a cationic cavity with host-guest interactions. Such red-shifts have been previously observed for radical cation spectra associated with poly-aromatic hydrocarbons inside the Cage[26]. Thus, the TA features could be assigned to the formation and decay of BTMC radical cation inside cavity. The entire ESA decays by 100 ps where there is a change in the absorption feature, and by 300 ps we see that there's a very low oscillator strength absorption remaining in the blue side of the probe region from 440 nm to 500 nm.

In order to test a possible protonation/deprotonation step after the radical cation formation, we also measured the TA traces for BTMC⊂Cage in D_2O (Figure 3b). We find that exactly similar features were obtained although with a slightly modified kinetics. The inherent dynamics of states were deconvoluted from the entire TA spectral dataset using a three-state sequential model by singular value decomposition (SVD) to obtain the lifetime and absorption spectra of each species (details in supporting information). Figure 3c and 3d shows the evolution associated spectra (EAS) of all the components and their respective lifetimes in both H_2O and D_2O. The green spectral trace represents the host-guest complex local excited (LE) state whose lifetime is ~300 fs. Although one would expect that the 400 nm photo-excitation leads to S_1 of the BTMC molecule but the electronic structure of the incarcerated BTMC molecule could have charge transfer character already mixed in. Therefore, in all subsequent discussions in the manuscript, we assigned the LE to have a CT character inside the Cage, and its evolution to

View Article Online
DOI: 10.1039/D5SC05247E

radical cation state only arises after a formal electron transfer (ET) to the Cage. This ET timescale of ~300 fs is independent of solvent isotope effect. The red trace shows radical cation absorption of BTMC⊂Cage with a lifetime of ~60 ps in H_2O. Interestingly, spectrum for the radical cation state bears close similarity to the spectrum assigned for the LE state which indicates that the initial excited state has a strong hybridization of the BTMC and the Cage molecular orbitals due to charge transfer character. The decay of this radical cation is expected to be via deprotonation of the -CH_3 group of BTMC molecule, thereby giving rise to the neutral C-site radical. This deprotonation happens due to the presence of pre-organized solvent shell of water molecules which acts as a proton acceptor. Hence, a secondary KIE is expected when we change the solvent from H_2O to D_2O with dependence of BTMC radical cation lifetime.

View Article Online
DOI: 10.1039/D5SC05247E

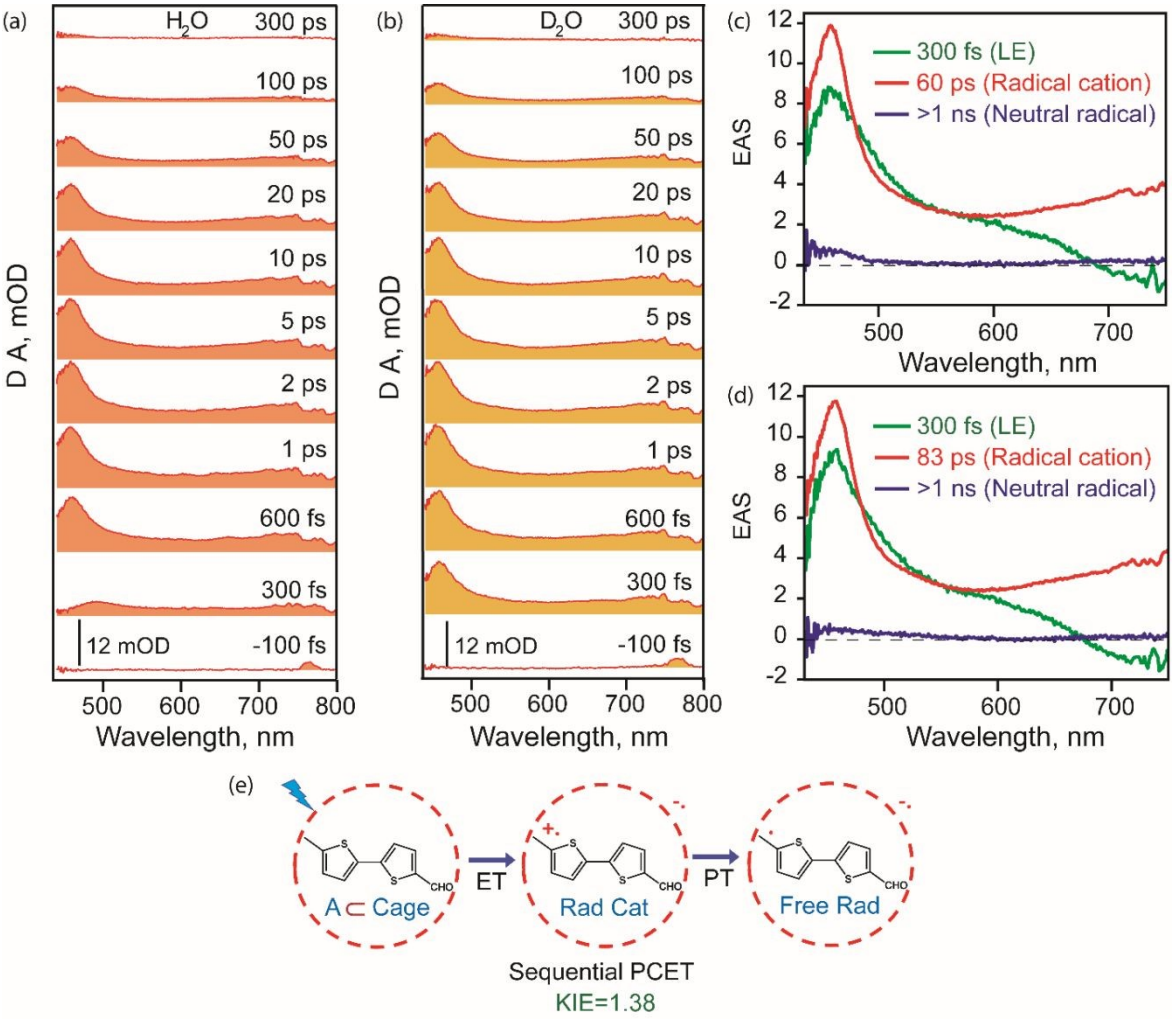

Figure 3: Transient Absorption Spectra and Dynamics. Fs-ns transient absorption of BTMC⊂Cage in the probe region of 430-800 nm on 400 nm excitation in (a) H_2O and (b) D_2O. SVD of the entire spectra into three state sequential model showing the evolution associated spectra in (c) H_2O and (d) D_2O. (e) Reaction mechanism of sequential PCET of BTMC⊂Cage as observed from fs-ns TA.

Although the initial electron transfer timescale of 300 fs remains same in D_2O (green trace in Figure 3d), the radical cation (red trace in Figure 3d) lifetime is now elongated to ~83 ps showing a secondary KIE of 1.38. Such a KIE is expected for the sequential PCET reaction [49]. A single point kinetics clearly showing slower decay of radical cation state at 460 nm in D_2O vs H_2O is shown in Figure S10. Thus, indeed there is a deprotonation step involved as seen from the H_2O vs D_2O dependence of the dynamics of BTMC radical cation in cavity. In both H_2O and D_2O there is a long-lived component (blue trace in Figure 3c and 3d) with a low oscillator

View Article Online
DOI: 10.1039/D5SC05247E

strength which is presumably the BTMC neutral radical spectrum inside the Cage cavity. The global analysis along with single point kinetics showing the quality of data fitting presented in Figure S11 and Figure S12.

We also probed the NIR region to observe the extent of the radical cation spectrum and to monitor the host-guest CT state dynamics. The transient absorption in the NIR region is shown in Figure S13. Evolution in the absorption spectra is shown from negative 100 fs to 300 ps in H_2O. We find a blue shift of the entire spectra with time. This feature in the NIR region has been assigned to a coupled host-guest radical cation and radical anion state based on previous work[24]. The blue shift of the transient spectrum describes the solvent reorganization in the host-guest charge transfer excited state. A single point kinetics at 880 nm of the TA data (Figure S13, b and c) shows a rise time of 1.55 ps which is the solvent reorganization timescale in H_2O and 1.77 ps in D_2O. A similar KIE is seen in the decay of the radical cation state showing deprotonation. Thus, from our TA measurements, we conclude that upon excitation of the host-guest complex with the 400 nm excitation there is an electron transfer representing host-guest charge transfer with ~300 fs timescale which gives rise to the radical cation state which then undergoes deprotonation showing a secondary KIE of 1.38 to give a neutral radical state. Figure 3e shows the probable pathway for radical formation through steps of electron transfer and proton transfer as also previously observed in such host guest systems. Thus, an ET followed by a PT which shows significant secondary kinetic isotope effect (KIE) marks for a sequential PCET mechanism.

In order to ascertain that the excited state dynamics arises indeed due to charge transfer process from confined BTMC molecule, excited state dynamics of free BTMC in $CHCl_3$ was studied after photoexcitation. From the steady-state absorption and emission spectra of BTMC in

View Article Online
DOI: 10.1039/D5SC05247E

$CHCl_3$ (Figure S5), we see a strong emission of the free molecule with emission maxima at 436 nm. The fluorescence lifetime as measured by TCSPC with an IRF of ~60 ps (Figure S14) shows a decay of 1.39 ns for an emissive state that rises with a ~57 ps time-constant. The data indicates that the local S_1 state in BTMC is long lived till 1.39 ns with an internal conversion timescale of 57 ps within singlet states. Broadband transient absorption measurement of BTMC in $CHCl_3$ (Figure S15) shows a rise time of ~24 ps in the ESA which subsequently leads to a biexponential decay with time constants of 1.2 ns (53%) and >2 ns (47%) (single point kinetics in Figure S16). The ~24 ps timescale is the same process that was clocked by TCSPC with a much poor time resolution. It is well known for bithiophene frameworks that intramolecular charge transfer states[33, 50] can form in tens of picoseconds which can be polarity sensitive. Therefore, the rise time of ~24 ps which apparently corresponds to evolution to an emissive singlet state which is attributed to planarization of the bithiophene backbone as well as solvent reorganization on the excited state. The longer timescale dynamics were probed using nanosecond-microsecond transient absorption spectroscopy. Figure S17 shows the spectra collected between 1 nanosecond to 300 nanoseconds which is a signature of long-lived triplet state. Single point kinetics at 480 nm shows a biexponential decay of first a singlet state decay of 1.35 ns while a triplet state is observed with 224 ns lifetime (Figure S18). The formation of BTMC triplets in $CHCl_3$ contrasts to the dynamics of the sequential PCET pathway of BTMC□Cage solution which ultimately leads to C-H bond photoactivation.

FSRS dynamics during C-H bond activation: To watch the structural changes as the sp^3 -CH_3 site evolves to sp^2 -$\dot{C}H_2$ radical, we carry out FSRS to capture the Raman snapshots of the photoinduced sequential PCET chemistry. We assigned all the ground state Raman features of the host-guest complex using spontaneous CW Raman measurements. Raman spectra of free

View Article Online
DOI: 10.1039/D5SC05247E

Cage and BTMC□Cage were recorded under CW laser irradiation of 488 nm to assign the Cage modes,[19] and the BTMC molecular modes inside the cavity-confinement in ground state (Figure S19). We separately collected the stimulated Raman spectrum with 814 nm Raman pump (additional information about stimulated Raman experiment is provided in SI) for both 5 mM BTMC in DCM (Figure 4a; black trace) and 5 mM Cage in H_2O (Figure 4b; blue trace) in the ground state (all analysis procedures are described in SI). In order to assign the normal modes in the ground state, electronic structure optimization along with normal mode analysis of BTMC was done using DFT at cam-B3LYP/6-31g(d) while the Cage modes were already established from previous work[19]. Figure 4a shows the ground state stimulated Raman spectrum for the BTMC and its normal mode description (Figure S20) with the most intense Raman modes. In figure 4b, the ground state stimulated Raman spectrum of BTMC□Cage complex was then fitted to Gaussian peak fits to get a fitted spectrum (red line in Figure 4b). The 1475 cm^{-1} mode arises from the symmetric C=C stretching of the thiophene rings while both the 1425 cm^{-1} and 1557 cm^{-1} modes come from asymmetric C=C stretching of the thiophene rings (Figure 4a and Figure S20). The 1668 cm^{-1} mode is assigned to the C=O stretching of the aldehyde group. Many of the BTMC modes inside the cavity were prominently observed with 1472 cm^{-1} being the highest Raman active mode (Figure 4b). This mode however was 3 cm^{-1} red-shifted potentially due to the interactions with the cationic nanocage. In addition, the asymmetric C=C stretch was 2 cm^{-1} red-shifted while the 1655 cm^{-1} mode assigned to the C=O stretch was 13 cm^{-1} red-shifted from the observed frequency in DCM. The large red-shift in the C=O stretch arises from the hydrogen bonding interactions[19] of the aldehyde group with the surrounding water molecules that may be at the interface of the pores in the cavity.

View Article Online
DOI: 10.1039/D5SC05247E

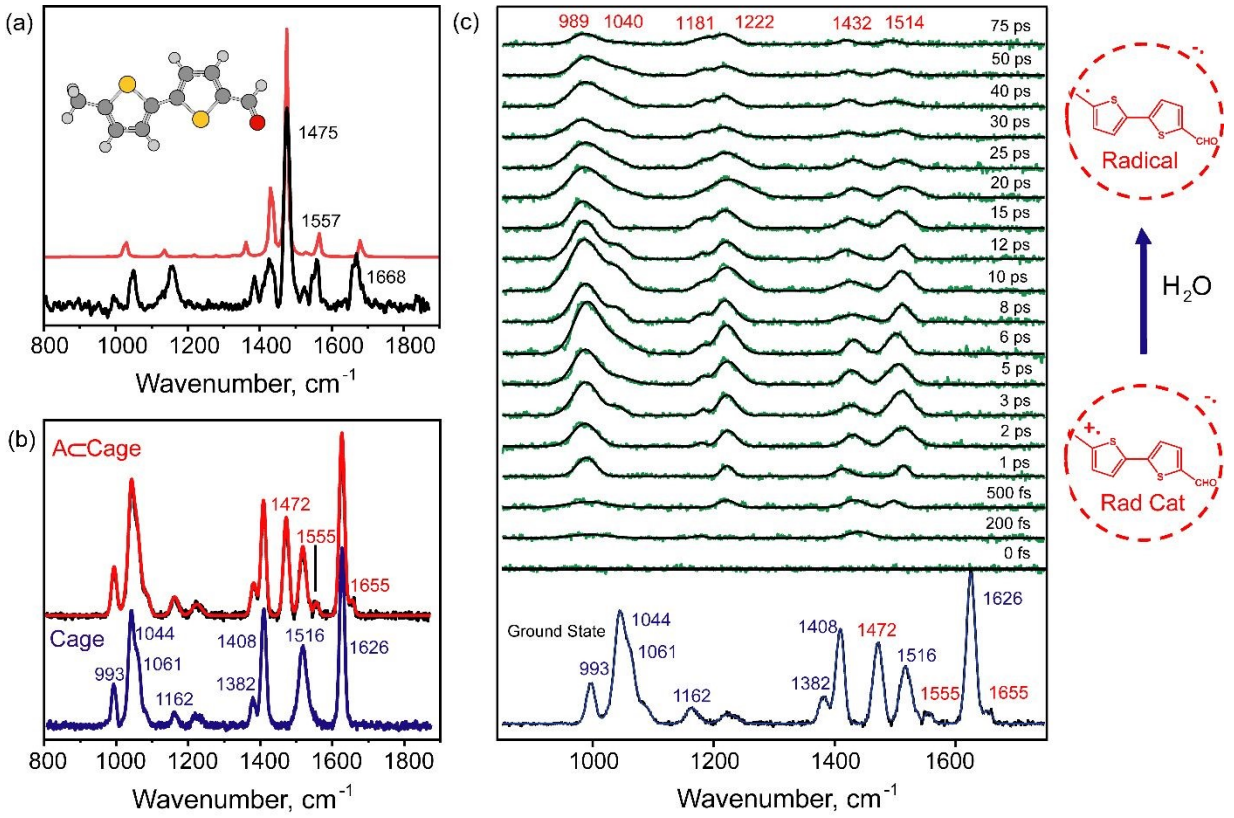

Figure 4: Transient Raman Snapshots of C-H bond Breaking. (a) The ground state stimulated Raman spectrum of the free BTMC in dichloromethane (DCM) is compared to the computational Raman spectrum. The principal modes are all marked. (b) Ground state stimulated Raman spectra of only Cage and BTMC incarcerated inside the Cage; the latter shows both the Raman features of the guest and the Cage. (c) Resonance selective transient stimulated Raman spectra of BTMC radical cation as it undergoes sequential proton-coupled electron transfer.

To understand the excited state structural changes associated with the steps of radical cation formation and its evolution to a neutral radical state through sequential PCET, time-resolved stimulated Raman spectra (see details in SI) were recorded subsequent to 400 nm femtosecond pump pulse excitation. The Raman excitation pulse was kept at 814 nm which was at pre-resonance with the excited state absorption of the radical cation feature at ~750 nm extending up to NIR region. This ensures that the resonance Raman features of the radical cation state will dominate over all other modes including the Cage features. Figure 4c shows the evolution of the excited state FSRS spectra at various time delays. The excited state Raman

View Article Online
DOI: 10.1039/D5SC05247E

features were extracted after few steps of data handling which involved ground state removal by 1:1 subtraction and baseline correction as elaborated in supporting information. We observe that the excited Raman peaks take time to build up after the formal t=0 after photoexcitation. The initial time traces from 200 fs to 3 ps in Figure 4c show spectral features in three distinct regions: (a) features at 1514 cm^{-1} and 1432 cm^{-1}, (b) a feature at ~1215 cm^{-1} and (c) a broad feature at ~990 cm^{-1}. It is well known that the high frequency modes around 1400-1600 cm^{-1} arises from the C=C stretching frequencies of the bithiophene ring radical cation state as reported in literature [48]. The sub-picosecond risetime of these features indicates that stimulated Raman spectral features of the neutral excited state (LE) are potentially buried under the resonance-enhanced radical cation Raman spectra although we did carry out singular value decomposition to extract the LE features. The lower frequency modes at 989 cm^{-1} and 1222 cm^{-1} are assigned to C-H bending modes coupled to the C=C stretches. In the later time points from 10 ps to 75 ps, we observe intensity decay of the high frequency modes while new lower frequency modes seem to appear at 1040 and 1181 cm^{-1}. The observed changes in the relative spectral intensities and frequencies of the modes clearly indicate structural evolution of the bithiophene backbone during the C-H bond activation chemistry.

In order to analyze the dynamics of the modes, we carried out kinetic fits for the major peaks as well as global fits to the entire FSRS data. The most intense Raman modes at 1432 and 1514 cm^{-1} in Figure 4c potentially mark the rise and decay of radical cation state. Figure S21 shows the decay of the integrated areas of the peaks at 1432 and 1514 cm^{-1} respectively. A rise time of ~0.6 ps and a mono-exponential decay of 30 ± 10 ps were observed for the integrated peak area of the 1514 cm^{-1} mode. It should be noted here that the large errors on the fits reflect the peak area scatter on the obtained experimental data. The 1432 cm^{-1} mode however showed a

View Article Online
DOI: 10.1039/D5SC05247E

rise-time of 2 ps with a decay of 40 ± 10 ps. Thus, the dynamics of our FSRS data shows a dispersion of timescales for both the modes while indicating perhaps a faster 30-40 ps decay of radical cation as compared to the ~60 ps decay observed from our TA experiments.

To increase the robustness of timescales associated with radical cation decay from FSRS experiments compared to TA, we globally analyzed the FSRS data using 3-state sequential model analogous to the TA dataset. We found that we can globally fit the data with 3 individual components, and extract stimulated Raman spectra of the host-guest complex LE state, the radical cation state and the neutral radical state. We find that for LE state lifetime of 2-3 ps fits well to the data while being similar to the TA data. Our fits for the radical cation show that when radical cation lifetimes are varied between 14-30 ps, the obtained deconvoluted stimulated Raman spectra of all the three states are robust. The stimulated Raman spectrum of the LE, radical cation and neutral radical states are plotted in Figure 5. Both single pointkinetics and kinetics from SVD are shown in supporting information Figure S21 and S22. If we constrain the radical cation lifetime beyond 30 ps, we immediately observe that the fits are not good enough as well as the deconvolved Raman spectra has baseline artifacts since the FSRS dataset beyond 75 ps has low S/N ratio. The deconvoluted radical cation Raman spectrum is characterized by intense modes at 985 cm^{-1}, 1216 cm^{-1}, 1430 cm^{-1} and 1510 cm^{-1}. This spectrum has modes which compares well with the experimental resonance Raman data of the bithiophene radical cation spectrum obtained by Jensen et al using nanosecond time-resolved Raman spectroscopy with 425 nm excitation at low temperature[47]. Peaks at 1535, 1435, 1358, 1276, 1219, 1166, 1070 and 979 cm^{-1} respectively characterize the experimental radical cation Raman spectrum from previous work. Our peaks at 1510, 1430, 1216, 1186, 1046 and 985 cm^{-1} make the FSRS obtained spectra a reasonable match although our spectral resolution is ~16 cm^{-1} while the peak widths are ~30-40

View Article Online
DOI: 10.1039/D5SC05247E

cm^{-1}. It should be noted that CT interactions with Cage as well as interaction with water potentially can shift the mode frequencies in radical cation state although most of the modes have similar peak positions. The extracted neutral radical Raman spectrum resembles the spectra in the raw FSRS data which remains after 30 ps characterized by two main features at 972 cm^{-1} with a 1022 cm^{-1} shoulder and at 1197 cm^{-1} as the major modes with low intensity transitions at 1420 cm^{-1} and 1480 cm^{-1} respectively. It is reasonably clear that removal of the proton from the -CH_3 group would extend the conjugation of the thiophene rings to the -CH_2 group, thereby enhancing the relative intensity of the C-H in-plane bends at ~900-1100 cm^{-1} region.

Interestingly, we could also deduce an LE state Raman spectra which seems to have very similar to the characteristic features to the radical cation Raman spectrum although with lower signal-to-noise ratio. Thematically, it matched well to our TA data which also shows spectral similarity of the initial LE state which already has a charge transfer or a partial radical cation character. In fact, both FSRS and TA suggest that CT interactions of BTMC with the Cage sufficiently modifies the excited states accesses with 400 nm pump pulse so that we see the precursor CT state before the radical cation formation. Since resonance FSRS dominates along with larger Raman cross section of a potentially planar radical cation framework, the radical cation spectra is more sensitively detected and dominates any observable LE state of the host-guest complex with neutral BTMC. In summary, using global analysis, we robustly enunciate the Raman spectrum of the proton-abstracted neutral radical which is very distinct from the radical cation state marking the loss of the proton from the -CH_3 group. It also uncovered that the proton transfer (PT) timescales can be heterogeneous in tens of picoseconds as determined by the combination of femtosecond stimulated Raman and transient absorption spectroscopies.

View Article Online
DOI: 10.1039/D5SC05247E

In an attempt to assign the excited state modes, electronic structure optimization with normal mode analysis was done for BTMC in gas phase since vibrational calculations for host-guest CT states are computationally challenging. For best comparison, we still computed the Raman spectrum of the locally excited S_1 state for BTMC molecules, an artificially created BTMC radical cation in its D_0 and D_1 states, and the corresponding neutral radical in its D_0 and D_1 states respectively. We compared our FSRS data to the computed Raman spectra for the D_0 state since it is energetically accessible from the LE of the BTMC molecule. The changes in the bond lengths and dihedral angles for all the optimized geometries are given in Figure S23. The computed Raman spectra for S_1 of BTMC, D_0/D_1 of radical cation BTMC and D_0/D_1 of BTMC radical are compared while the comparison with ground state is shown in Figure S24. As expected, the extracted FSRS spectrum of the LE state does not match the computational vibrational spectra in the S_1 state of isolated neutral BTMC molecule. This is observed because upon incarceration of BTMC in Cage and excitation with light a charge transfer state is formed. In fact, S_1 Raman spectrum should have shown just one intense C=C stretching peak of 1524 cm^{-1} while the rest of the modes have low polarizability.

The computed Raman spectrum of the gas-phase radical cation D_0 state has intense modes at 1505 cm^{-1} for C=C stretch (Figure S24b) along with a mode at 1710 cm^{-1} for the carbonyl group. Along with these modes, we also find lower polarizability for the Raman lines associated with C=C stretching at 1380 cm^{-1}, 1404 cm^{-1} and 1460 cm^{-1} on two unsymmetric thiophene rings. Mode at 1160 cm^{-1} corresponds to the C-H in plane bending mode coupled to C=C stretch of the backbone while weak bands are seen at 1060 cm^{-1} region also. A direct comparison of the SVD extracted Raman data suggests that some experimental FSRS peaks could be explained by the gas-phase computed D_0 state although most of the modes are

View Article Online
DOI: 10.1039/D5SC05247E

supported by the experimental data obtained by Jensen et al.[47] Therefore we believe a more accurate calculation with BTMC incarcerated inside the Cage having an anion radical is required to completely simulate the experimental BTMC radical cation FSRS spectrum.

For the neutral radical D_0 state computations, we see enhanced Raman intensities at 1017 cm^{-1}, 1175 cm^{-1}, 1280 cm^{-1} and 1367 cm^{-1} respectively (Figure S24c). Additionally, less intense peaks at 1428 cm^{-1} and at 1480 cm^{-1} are also observed. The normal modes with the displacement vectors of the most intense Raman modes in BTMC neutral radical D_0 state are shown in Figure S25. We find that our FSRS data does not completely align with the predicted D_0 state of the free BTMC neutral radical. Interestingly, we cannot rule out the energy accessibility of the D_1 state from the D_0 state for Cage-confined BTMC neutral radical. We hypothesize that due to strong interactions with the Cage anion radical as well as specific water interactions with the BTMC backbone, the D_1 state can be stabilized in confinement. We therefore find it reasonable to compare the computed D_1 Raman spectrum to our obtained neutral radical FSRS spectrum at long time delays especially from 30-60 ps. We find that the major peaks at 996 cm^{-1} and 1155 cm^{-1} in the computations (normal modes shown in Figure S25) match favorably to our features at 972 cm^{-1} and 1197 cm^{-1} while smaller features at 1390 cm^{-1} and 1450 cm^{-1} are also observed similar to our SVD extracted features at 1420 cm^{-1} and 1480 cm^{-1} respectively. We find that our experimental FSRS spectra of the neutral radical indeed matches better with the computed D_1 state although we cannot track its decay to the final D_0 state in the FSRS experiment. The geometry change results in planarization of the bithiophene framework either in its D_1 or D_0 state although further high-level calculations in future are required to compute the Raman spectrum of the BTMC radical states when incarcerated inside the Cage in its anion radical state. We therefore conclude that the deprotonation on the $-CH_3$ site and formation of a $-\dot{C}H_2$ radical being

View Article Online
DOI: 10.1039/D5SC05247E

visualized by FSRS, brings in a double bond character to the C_9-C_{10} bond which now being in conjugation with the bithiophene backbone enhances the Raman intensities of the adjacent C-H bending modes. The decay of the high frequency C=C stretching modes and rise of C-H bending modes mark the formation of the neutral radical or the activated Carbon-site.

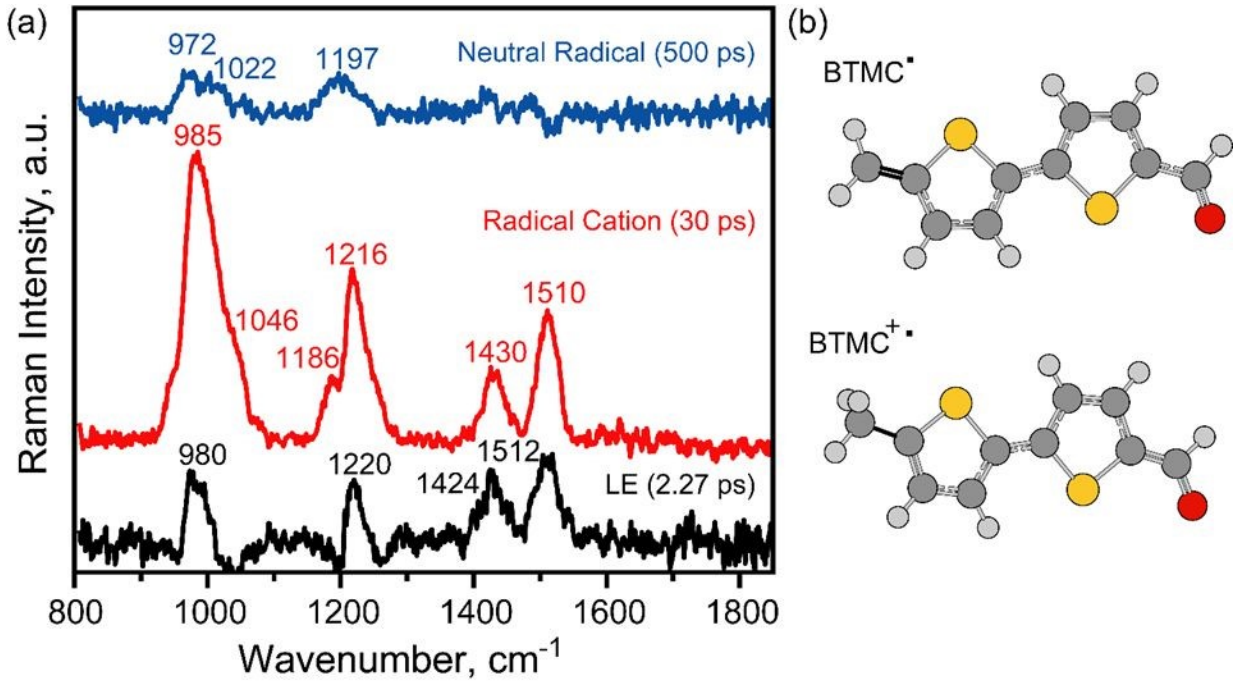

Figure 5: (a) SVD of FSRS data to show distinct features of LE, radical cation and neutral radical modes. The spectral traces have been offset for clarity. (b) Structural change of BTMC from radical cation to neutral radical state through PCET.

Figure 5 shows the structural change in this excited state pathway along with the evolution in the Raman spectra from BTMC in LE to the radical cation and subsequently to the neutral radical state. The optimized structures' nuclear coordinates for the ground state and first excited state of radical cation and radical are shown in Table S1-6. We observe that the thiophene rings in the ground state for BTMC are out of plane with a S_2-C_6-C_5-S_1 dihedral being 169.72°. Typically for the free BTMC molecule, in the first excited state there is partial attainment of planarity and a subsequent increase of π-conjugation in the bithiophene backbone as seen from the BTMC S_1 bond lengths and dihedral. Although in our case S_1 is not observed

View Article Online
DOI: 10.1039/D5SC05247E

due to increased CT character once the BTMC is confined inside the Cage which is an electron acceptor. In the radical cation state, which is a one-electron removed species from BTMC there is even higher π-delocalization and planarity in the ground D_0 or even in D_1 state. On analyzing the neutral radical structure as compared to the radical cation the deprotonation on the $–CH_3$ group forms a $-\dot{C}H_2$ sp^2 site which can now have a partial double bond character due to conjugation with the bithiophene rings. This is depicted in the shortening of C_9-C_{10} bond lengths in Figure S23 in case of the neutral radical state.

An alternate viewpoint can be proposed that involves Raman detection of Cage anion radical modes mixed in with the evolution of the BTMC radical cation to the BTMC neutral radical features. However, a careful analysis of the Cage anion radical modes (shown in Figure S26) with respect to neutral Cage modes shows that there will be multiple tripyridyltriazine (TPT)-centric ligand modes expected in between 1300 to 1700 cm^{-1} with reasonable intensity including few beyond 1500 cm^{-1} which is not observed in our FSRS spectral evolution. Additionally, these TPT-centric modes should have a clear distinction in temporal decay dynamics compared to the BTMC radical cation modes which decay away in 14-30 ps. As the Cage anion radical should be observed throughout the BTMC evolution dynamics, we do not observe any such temporally distinct TPT-centric modes which could signify any detectable Cage anion radical modes. Taken together with resonance enhanced Raman signals of BTMC radical cation and neutral radical features, we rule out any possibility of Cage anion contributions to the FSRS evolution in tens of picoseconds.

View Article Online
DOI: 10.1039/D5SC05247E

FSRS dynamics and reaction coordinate: In summary, the FSRS data with all its assignments clearly indicates that the radical cation state can be discriminated using the Raman spectrum unlike the transient absorption data, where they appear similar with broad features although distinct oscillator strengths. Additionally, the differences in proton transfer timescales scored by

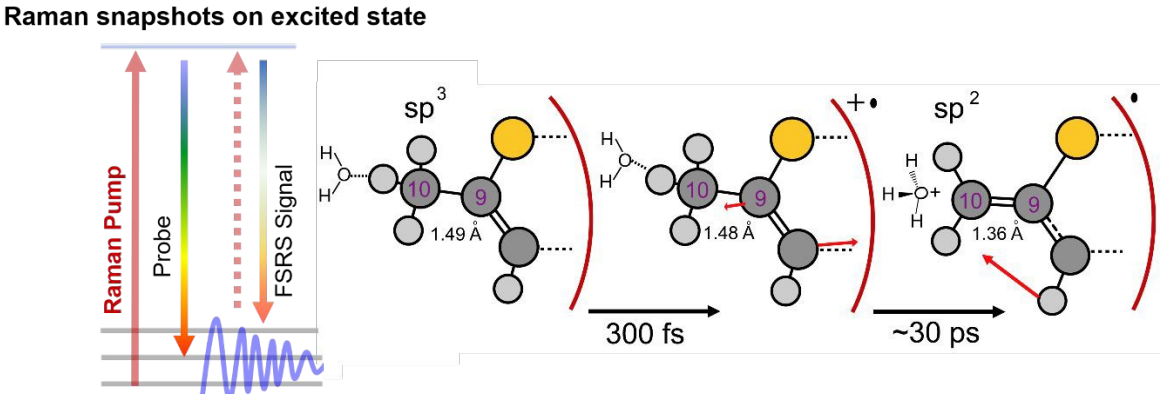

Figure 6: PCET dissected with excited state stimulated Raman. FSRS measurements reveal the structural dynamics of the C-H bond activation reaction. It proceeds through a radical cation intermediate whose structure evolves to the planar neutral radical confined inside a water-soluble nanocage.

FSRS is broadly between 14-30 ps, much faster than ~60 ps TA rates. To us, it suggests the possibility that in transient absorption the spectral changes accommodate both the deprotonation dynamics of formal C-H bond-breaking along with other associated structural relaxation, e.g. the equilibration of the incipient proton with the interacting water cluster. The difference in apparent timescales between FSRS and TAS arises fundamentally from the different observables probed by the two techniques. FSRS directly tracks the evolution of vibrational coherences and frequencies, which are sensitive to structural relaxation on the excited-state potential energy surface, and can be insensitive to changes in electronic oscillator strength. In contrast, TAS signals explicitly depend on the electronic transition strengths and the populations. Thus, changes in oscillator strength during relaxation can significantly alter TAS amplitudes and

View Article Online
DOI: 10.1039/D5SC05247E

kinetics without reflecting a change in the underlying structural dynamics. Our results thus indicate that there can be heterogeneity of deprotonation rates in this host-guest CT system, and solely transient absorption signatures for interpreting proton transfer timescales may be insufficient. Therefore, it is best to complement the TA with time-resolved vibrational spectroscopy tools to disentangle the timescales of definite structural changes from the electronic state changes.

FSRS provides vibrational signatures of the structural change that occurs during the formation of neutral radical which has an increased backbone conjugation compared to the radical cation state. The C_9-C_{10} bond attains a partial double bond character and hence the tetrahedral carbon becomes planar after deprotonation. This is being marked by the rise of the C-H bending modes intensity adjacent to the methyl group. Interestingly the ~60 ps deprotonation dynamics from transient absorption spectroscopy has a KIE of ~1.4 when D_2O replaces the solvent water. As FSRS scores for a 14-30 ps proton dissociation timescale, we reinterpret the transient absorption dynamics to include not only the fundamental deprotonation but it also enunciates the role of proton hopping within the associated water cluster in stabilizing the neutral radical state. Traditionally, KIE in PCET provides information of the distances associated with the donor and acceptor, with small KIEs of ~1.1 representing short proton hopping distances. In future, we plan to mechanistically understand how the extensive hopping amongst the water cluster which pushes the value to ~1.4 using detailed molecular dynamics simulations which include solvation of the host-guest complexes. We, therefore, conclude that water cluster rearrangements around the BTMC C_{10}-H bond should be a crucial reaction-coordinate enabling the proton stabilization as a base after C-H bond cleavage from the radical cation. Our measurements fall in line with the work of Hammes-Schiffer and co-workers who had predicted

View Article Online
DOI: 10.1039/D5SC05247E

that excited state sequential PCET reaction should also have a dominating solvent rearrangement coordinate. We believe that in future in-depth multidimensional 2D electronic-vibrational spectroscopy along with impulsive excitation might unravel all the low-frequency modes associated with formation of the radical cation state and ensuing deprotonation on the excited state. Additionally, as mentioned previously the FSRS mode frequencies in radical cation and neutral radical states cannot directly be compared to gas phase calculations of free BTMC molecules, and detailed computations considering all atoms explicitly are required for the host-guest CT systems in future. Once these frequencies are computed, ab-initio molecular dynamics simulations could also reveal the rich water dynamics during the sequential PCET step that enables Cage-confined photoredox catalysis.

Recently, Fleming and co-workers have shown excited state PCET occurring via two reactive pathways of fast PCET (minor pathway of 4%) and a relaxed PCET (major pathway of 96%) in a bio-mimetic benzimidazole-phenolpentafluorophenylporphyrin (BIPPF15) complex through two-dimensional electronic−vibrational spectroscopy[51]. Their work illustrates that in cases where the proton acceptor and electron acceptors are in the same framework heterogenous pathways for PCET may exist making it difficult to use a single-reaction coordinate description. In contrast, we find that if a pre-organized water cluster interacts with the guest inside the cavity, one can have a single PCET pathway with separate electron and proton acceptor. Our work also contrasts with the concerted PCET pathways in excited state described by Mayer and co-workers in the inverted Marcus region[52]. We thereby have generated an optimized situation for non-equilibrium PCET reaction inside a cavity that can be exploited for high efficiency C-H bond functionalization reactions in water[25].The significance of pre-organized water cluster therefore is to provide functional water molecules that act as a co-factor to the actual cationic nanocage

View Article Online
DOI: 10.1039/D5SC05247E

catalyst for removing charge buildup by providing a proton-transfer network in ~10-100 picoseconds timescale. Our photoredox strategy here complements the classical diffusion-based paradigm initially popularized by Macmillan and co-workers and now used extensively[53].

Conclusions

To summarize we track the primary steps of ultrafast C–H bond photoactivation within a water-soluble supramolecular cavity using a synergistic combination of transient absorption and femtosecond stimulated Raman spectroscopy (FSRS). As Figure 6 shows we demonstrate selective aldehyde formation at a terminal $–CH_3$ group appended to a bithiophene backbone via a well-defined photoinduced proton-coupled electron transfer (PCET) mechanism along a host–guest charge-transfer (CT) potential energy surface. Rich vibrational dynamics—particularly thiophene C–H in-plane bending modes coupled with C=C stretches—provide unequivocal evidence of C–H bond breaking step, as the radical cation state is resonantly enhanced in our FSRS data. The emergence of shifted vibrational modes following deprotonation marks the formation of the neutral radical within ~14-30 ps which is certainly faster than changes observed by probing the excited state absorption features via transient absorption spectroscopy which are sensitive to population decay, relaxation and oscillator strength changes. A pronounced secondary kinetic isotope effect in D_2O, along with insights from the vibrational "Raman movie" highlights the critical role of closely interacting water cluster in facilitating deprotonation while potentially highlighting the heterogeneity in the proton transfer step. Our work therefore provides the first structural visualization of an ultrafast PCET-triggered C–H activation event, revealing how substrate interaction with the water clusters stabilizes on-pathway intermediates in real time. We envision that the synthetic community would use modular host-guest strategy for

View Article Online
DOI: 10.1039/D5SC05247E

harnessing photoinduced PCET reactions in aqueous environments for targeted organic transformations.

Supplementary information: Description of the materials and experimental methods, additional figures pertaining to the experiments are given in supporting information.

Author Contributions: J.D. conceived the research, and planned the initial experiments with A.D. and S.P. Original synthesis, characterization, time-resolved spectroscopy and FSRS measurements were carried out by S.P. while the data was analyzed by S.P. with help from J.D. A.D. carried out the initial work of characterizing host-guest complexes of bithiophene substrates for the FSRS measurements. Shashi carried out additional characterization of the host-guest complex and provided control photoreactivity experiments. The electronic structure calculations along with Raman calculations for BTMC were performed by S.P. Computations for extracting the Raman spectrum of the neutral Cage and its anion radical was performed by D.M. The manuscript was written by S.P., Shashi, A.D. and J.D. with contributions from D.M. All the co-authors discussed the scientific content in detail and agreed with the final form of the manuscript.

ACKNOWLEDGMENTS

S.P, Shashi, A.D and J.D. acknowledge support from the Department of Atomic Energy (DAE), Government of India, under Project no. 12-R&D-TFR-5.10-0100. D.M. acknowledges funding from the Ramon y Cajal grant RYC2020-029863-I through the Instituto de Ciencia de Materiales de Madrid, Consejo Superior de Investigaciones Cientificas (CSIC-ICMM), PIE grant from CSIC-ICMM (20226AT001), and the Spanish Ministerio de Ciencia, Innovacion y Universidades grants (PID2019-111086RA-I00, TED2021-1327 57B–I00, PID2022-143013OB-I00, CNS2023-145046). The authors would like to specially thank Prof. Ayan Datta (IACS Kolkata) and Chandralekha (IACS Kolkata) for their helpful discussions and collaborative ideas.

View Article Online
DOI: 10.1039/D5SC05247E

We also thank Prof. Vamsee Voora (TIFR Mumbai) for discussion on electronic structure calculations. The authors acknowledge the discussions with Dr. Arup Kundu, Dr. Dipin Tomer, Dr. Debojyoti Roy, Dr. Kishan Yadav (TIFR Mumbai). The authors thank Mrs. Mamta Kallianpur (TIFR Mumbai) for help in the TCSPC measurements.

Corresponding Author(s)

Jyotishman Dasgupta − Department of Chemical Sciences, Tata Institute of Fundamental Research, Mumbai 400005, India; orcid.org/0000-0003-4607-653X; Email: dasgupta@tifr.res.in

References:

(1) Zewail, A. H. Laser selective chemistry—is it possible? *Physics Today* **1980**, *33* (11), 27–33.
(2) Vos, M. H.; Rappaport, F.; Lambry, J.-C.; Breton, J.; Martin, J.-L. Visualization of coherent nuclear motion in a membrane protein by femtosecond spectroscopy. *Nature* **1993**, *363* (6427), 320–325.
(3) Zewail, A. H. Femtochemistry: Atomic-scale dynamics of the chemical bond. *The Journal of Physical Chemistry A* **2000**, *104* (24), 5660–5694.
(4) Park, S. T.; Feenstra, J. S.; Zewail, A. H. Ultrafast electron diffraction: Excited state structures and chemistries of aromatic carbonyls. *The Journal of chemical physics* **2006**, *124* (17).
(5) Zhang, M.; Zhang, S.; Xiong, Y.; Zhang, H.; Ischenko, A. A.; Vendrell, O.; Dong, X.; Mu, X.; Centurion, M.; Xu, H. Quantum state tomography of molecules by ultrafast diffraction. *Nature communications* **2021**, *12* (1), 5441.
(6) Marangos, J. The measurement of ultrafast electronic and structural dynamics with X-rays. The Royal Society Publishing: 2019; Vol. 377, p 20170481.
(7) Zhang, Z.; Tanaka, K.; Yu, J.-Q. Remote site-selective C–H activation directed by a catalytic bifunctional template. *Nature* **2017**, *543* (7646), 538–542.
(8) Goswami, N.; Bhattacharya, T.; Maiti, D. Transient directing ligands for selective metal-catalysed C–H activation. *Nature Reviews Chemistry* **2021**, *5* (9), 646–659.
(9) Ramadoss, B.; Jin, Y.; Asako, S.; Ilies, L. Remote steric control for undirected meta-selective C–H activation of arenes. *Science* **2022**, *375* (6581), 658–663.
(10) Trost, B. M. The atom economy—a search for synthetic efficiency. *Science* **1991**, *254* (5037), 1471–1477.
(11) Marson, C. M. Multicomponent and sequential organocatalytic reactions: diversity with atom-economy and enantiocontrol. *Chemical Society Reviews* **2012**, *41* (23), 7712–7722.
(12) Heck, R. F.; Nolley Jr, J. Palladium-catalyzed vinylic hydrogen substitution reactions with aryl, benzyl, and styryl halides. *The Journal of organic chemistry* **1972**, *37* (14), 2320–2322.
(13) Johansson Seechurn, C. C.; Kitching, M. O.; Colacot, T. J.; Snieckus, V. Palladium-catalyzed cross-coupling: a historical contextual perspective to the 2010 Nobel Prize. *Angewandte Chemie International Edition* **2012**, *51* (21), 5062–5085.
(14) Jay, R. M.; Banerjee, A.; Leitner, T.; Wang, R.-P.; Harich, J.; Stefanuik, R.; Wikmark, H.; Coates, M. R.; Beale, E. V.; Kabanova, V. Tracking C–H activation with orbital resolution. *Science* **2023**, *380* (6648), 955–960.
(15) Jun, C.-H. Transition metal-catalyzed carbon–carbon bond activation. *Chemical Society Reviews* **2004**, *33* (9), 610–618.
(16) Mayer, J. M. Proton-coupled electron transfer: a reaction chemist's view. *Annu. Rev. Phys. Chem.* **2004**, *55*, 363–390.
(17) Weinberg, D. R.; Gagliardi, C. J.; Hull, J. F.; Murphy, C. F.; Kent, C. A.; Westlake, B. C.; Paul, A.; Ess, D. H.; McCafferty, D. G.; Meyer, T. J. Proton-coupled electron transfer. *Chemical Reviews* **2012**, *112* (7), 4016–4093.
(18) Cukier, R. I.; Nocera, D. G. Proton-coupled electron transfer. *Annual review of physical chemistry* **1998**, *49* (1), 337–369.

View Article Online
DOI: 10.1039/D5SC05247E

(19) Das, A.; Jha, A.; Gera, R.; Dasgupta, J. Photoinduced charge transfer state probes the dynamic water interaction with metal–organic nanocages. *The Journal of Physical Chemistry C* **2015**, *119* (36), 21234–21242.
(20) Barnes, J. C.; Juricek, M.; Strutt, N. L.; Frasconi, M.; Sampath, S.; Giesener, M. A.; McGrier, P. L.; Bruns, C. J.; Stern, C. L.; Sarjeant, A. A. ExBox: a polycyclic aromatic hydrocarbon scavenger. *Journal of the American Chemical Society* **2013**, *135* (1), 183–192.
(21) Klosterman, J. K.; Iwamura, M.; Tahara, T.; Fujita, M. Energy transfer in a mechanically trapped exciplex. *Journal of the American Chemical Society* **2009**, *131* (27), 9478–9479.
(22) Grommet, A. B.; Feller, M.; Klajn, R. Chemical reactivity under nanoconfinement. *Nature nanotechnology* **2020**, *15* (4), 256–271.
(23) Roy, D.; Paul, S.; Dasgupta, J. Visible light-mediated C (sp 3)–H bond functionalization inside an all-organic nanocavity. *Chemical Communications* **2023**, *59* (88), 13143–13146.
(24) Gera, R.; Das, A.; Jha, A.; Dasgupta, J. Light-induced proton-coupled electron transfer inside a nanocage. *Journal of the American Chemical Society* **2014**, *136* (45), 15909–15912.
(25) Roy, D.; Yadav, K. K.; Dasgupta, J. Host–Guest Charge-Transfer Mediated Photoredox Catalysis Inside Water-Soluble Nanocages. *Accounts of Chemical Research* **2025**, *58* (16), 2600–2612.
(26) Das, A.; Mandal, I.; Venkatramani, R.; Dasgupta, J. Ultrafast photoactivation of C─ H bonds inside water-soluble nanocages. *Science advances* **2019**, *5* (2), eaav4806.
(27) Hammes-Schiffer, S. Theory of proton-coupled electron transfer in energy conversion processes. *Accounts of Chemical Research* **2009**, *42* (12), 1881–1889.
(28) Hammes-Schiffer, S.; Stuchebrukhov, A. A. Theory of coupled electron and proton transfer reactions. *Chemical reviews* **2010**, *110* (12), 6939–6960.
(29) Schoenlein, R.; Peteanu, L.; Mathies, R.; Shank, C. The first step in vision: femtosecond isomerization of rhodopsin. *Science* **1991**, *254* (5030), 412–415.
(30) Fang, C.; Frontiera, R. R.; Tran, R.; Mathies, R. A. Mapping GFP structure evolution during proton transfer with femtosecond Raman spectroscopy. *Nature* **2009**, *462* (7270), 200–204.
(31) Batignani, G.; Ferrante, C.; Scopigno, T. Accessing excited state molecular vibrations by femtosecond stimulated Raman spectroscopy. *The Journal of Physical Chemistry Letters* **2020**, *11* (18), 7805–7813.
(32) Batignani, G.; Mai, E.; Fumero, G.; Mukamel, S.; Scopigno, T. Absolute excited state molecular geometries revealed by resonance Raman signals. *Nature communications* **2022**, *13* (1), 7770.
(33) Roy, P.; Jha, A.; Yasarapudi, V. B.; Ram, T.; Puttaraju, B.; Patil, S.; Dasgupta, J. Ultrafast bridge planarization in donor-π-acceptor copolymers drives intramolecular charge transfer. *Nature communications* **2017**, *8* (1), 1716.
(34) Provencher, F.; Bérubé, N.; Parker, A. W.; Greetham, G. M.; Towrie, M.; Hellmann, C.; Côté, M.; Stingelin, N.; Silva, C.; Hayes, S. C. Direct observation of ultrafast long-range charge separation at polymer–fullerene heterojunctions. *Nature communications* **2014**, *5* (1), 4288.
(35) Bragg, A. E.; Yu, W.; Zhou, J.; Magnanelli, T. Ultrafast Raman spectroscopy as a probe of local structure and dynamics in photoexcited conjugated materials. *The journal of physical chemistry letters* **2016**, *7* (19), 3990–4000.
(36) Dasgupta, J.; Frontiera, R. R.; Taylor, K. C.; Lagarias, J. C.; Mathies, R. A. Ultrafast excited-state isomerization in phytochrome revealed by femtosecond stimulated Raman spectroscopy. *Proceedings of the National Academy of Sciences* **2009**, *106* (6), 1784–1789.
(37) Oscar, B. G.; Chen, C.; Liu, W.; Zhu, L.; Fang, C. Dynamic Raman line shapes on an evolving excited-state landscape: Insights from tunable femtosecond stimulated Raman spectroscopy. *The Journal of Physical Chemistry A* **2017**, *121* (29), 5428–5441.
(38) Taylor, M. A.; Zhu, L.; Rozanov, N. D.; Stout, K. T.; Chen, C.; Fang, C. Delayed vibrational modulation of the solvated GFP chromophore into a conical intersection. *Physical Chemistry Chemical Physics* **2019**, *21* (19), 9728–9739.
(39) Kukura, P.; McCamant, D. W.; Mathies, R. A. Femtosecond stimulated Raman spectroscopy. *Annu. Rev. Phys. Chem.* **2007**, *58*, 461–488.
(40) So, R. C.; Carreon-Asok, A. C. Molecular design, synthetic strategies, and applications of cationic polythiophenes. *Chemical reviews* **2019**, *119* (21), 11442–11509.
(41) Flammini, S.; Di Sante, M.; Costantini, P. E.; Mattioli, E. J.; Marconi, A.; Turrini, E.; La Rosa, S.; Montrone, M.; Marforio, T. D.; Nigro, M. Oligothiophene-based photosensitizers with tunable push–pull architectures: design, synthesis and characterization. *Journal of Materials Chemistry B* **2025**, *13* (39), 12536–12545.
(42) Fujita, M.; Oguro, D.; Miyazawa, M.; Oka, H.; Yamaguchi, K.; Ogura, K. Self-assembly of ten molecules into nanometre-sized organic host frameworks. *Nature* **1995**, *378* (6556), 469–471.
(43) Wallace, T. J.; Baron, F. A. Solvent Effects in the Oxidation of Sulfur Compounds. The Base-Catalyzed Oxidation of Alkylthiophenes. *The Journal of Organic Chemistry* **1965**, *30* (10), 3520–3523.

View Article Online
DOI: 10.1039/D5SC05247E

(44) KING, W. J.; Nord, F. PREPARATION OF THIOPHENE-2-ALDEHYDE AND SOME SUBSTITUTED THIOPHENE ALDEHYDES1. *The Journal of Organic Chemistry* **1948**, *13* (5), 635–640.
(45) KING, W. J.; Nord, F. STUDIES IN THE THIOPHENE SERIES. V. WOLFF-KISHNER REDUCTIONS1, 2. *The Journal of Organic Chemistry* **1949**, *14* (4), 638–642.
(46) Furutani, Y.; Kandori, H.; Kawano, M.; Nakabayashi, K.; Yoshizawa, M.; Fujita, M. In situ spectroscopic, electrochemical, and theoretical studies of the photoinduced host− guest electron transfer that precedes unusual host-mediated alkane photooxidation. *Journal of the American Chemical Society* **2009**, *131* (13), 4764–4768.
(47) Keszthelyi, T.; Grage, M. M.-L.; Offersgaard, J. F.; Wilbrandt, R.; Svendsen, C.; Mortensen, O. S.; Pedersen, J. K.; Jensen, H. J. A. 2, 2 '-Bithiophene Radical Cation: An Experimental and Computational Study. *The Journal of Physical Chemistry A* **2000**, *104* (12), 2808–2823.
(48) Grage, M. M.-L.; Keszthelyi, T.; Offersgaard, J. F.; Wilbrandt, R. Bithiophene radical cation: resonance Raman spectroscopy and molecular orbital calculations. *Chemical physics letters* **1998**, *282* (2), 171–175.
(49) Tyburski, R.; Liu, T.; Glover, S. D.; Hammarström, L. Proton-coupled electron transfer guidelines, fair and square. *Journal of the American Chemical Society* **2021**, *143* (2), 560–576.
(50) Zhao, G. J.; Chen, R. K.; Sun, M. T.; Liu, J. Y.; Li, G. Y.; Gao, Y. L.; Han, K. L.; Yang, X. C.; Sun, L. Photoinduced Intramolecular Charge Transfer and S2 Fluorescence in Thiophene-π-Conjugated Donor–Acceptor Systems: Experimental and TDDFT Studies. *Chemistry–A European Journal* **2008**, *14* (23), 6935–6947.
(51) Yoneda, Y.; Mora, S. J.; Shee, J.; Wadsworth, B. L.; Arsenault, E. A.; Hait, D.; Kodis, G.; Gust, D.; Moore, G. F.; Moore, A. L. Electron–nuclear dynamics accompanying proton-coupled electron transfer. *Journal of the American Chemical Society* **2021**, *143* (8), 3104–3112.
(52) Parada, G. A.; Goldsmith, Z. K.; Kolmar, S.; Pettersson Rimgard, B.; Mercado, B. Q.; Hammarström, L.; Hammes-Schiffer, S.; Mayer, J. M. Concerted proton-electron transfer reactions in the Marcus inverted region. *Science* **2019**, *364* (6439), 471–475.
(53) Shaw, M. H.; Twilton, J.; MacMillan, D. W. Photoredox catalysis in organic chemistry. *The Journal of organic chemistry* **2016**, *81* (16), 6898–6926.

View Article Online
DOI: 10.1039/D5SC05247E

DATA AVAILABILITY STATEMENT

The data supporting this article have been included as part of the Supplementary Information.